Energy Analysis of Fleet Operations Using Green Liquid Hydrogen and Synthetic Kerosene

Conor Gallagher[1], Noah McCarthy[2], Charles Stuart[3], Stephen Spence[4]
Trinity College Dublin, the University of Dublin, Ireland

This study aims to determine the optimal fuel choice from a well-to-wake energy perspective by means of a comparative energy analysis of real-world fleet operations using green liquid hydrogen and synthetic sustainable aviation fuel. A calibrated Boeing 737-800NG model was developed using the SUAVE aircraft design tool, and a validated surrogate propulsion model was developed within NPSS and integrated into SUAVE. Three hydrogen aircraft, with various tank technology levels and an extended fuselage, were sized for the baseline design mission, maintaining fixed passenger capacity and design range. The in-flight energy performance of the hydrogen and sustainable aviation fuel aircraft were compared for the 29 real-world missions, in which the hydrogen aircraft yielded worse in-flight performance for all flights. However, when analysing the well-to-wake energy consumption and renewable electricity requirements, substantial energy savings could be obtained for the hydrogen aircraft, which may be desirable to reduce the significant strain placed on renewable electricity resources. Furthermore, it was found that a tank gravimetric efficiency of 50% was sufficient for superior performance of hydrogen aircraft against all SAF scenarios, further highlighting the potential of green hydrogen to minimise the energy demand of short-haul aviation over synthetic SAF in the context of decarbonisation.

I. Nomenclature

GW = Giga-Watt
ICAO = International Civil Aviation Organisation
L/D = Lift to Drag
LCOE = Levelised Cost of Electricity
LH2 = Liquid Hydrogen
MTOW = Maximum Take-Off Weight
MWh = Mega-Watt hours
NM = Nautical Miles
NPSS = Numerical Propulsion System Software
NS = North Sea
SAF = Sustainable Aviation Fuel
SLS = Sea-Level Static
SUAVE = Stanford University Aerospace Vehicle Environment
TOW = Take-Off Weight
TSFC = Thrust Specific Fuel Consumption
TWh = Terra-Watt hours
WtW = Well-to-Wake
VLM = Vortex-Lattice Method

$C_{D,p}$ = Fuselage parasite drag coefficient
C_f = Skin friction coefficient
k = Form factor
m = Mass
R_{fuel} = Fuel mass ratio
S_{ref} = Reference area

[1] Ph.D. Student, Department of Mechanical, Manufacturing and Biomedical Engineering.
[2] MAI Student, Department of Mechanical, Manufacturing and Biomedical Engineering.
[3] Assistant Professor, Department of Mechanical, Manufacturing and Biomedical Engineering.
[4] Professor, Department of Mechanical, Manufacturing and Biomedical Engineering.

II. Introduction

This study aims to determine the optimum fuel choice for aircraft based on a comparative 'Well-to-Wake' (WtW) analysis of fleet operations. Electrification has been accelerated in other transport modes in recent years, however fully-electric aircraft are simply infeasible to replace civil transport aircraft with the range and payloads required for airlines [1]. For the foreseeable future, aviation needs fuel – fuel that does not emit harmful emissions, while maintaining the high energy efficiency and safety margins demanded by the industry. Sustainable Aviation Fuel (SAF) and green liquid hydrogen are two potential solutions. Green hydrogen is produced through electrolysis of water using renewable electricity, whereas SAF can be produced via two distinct pathways; biofuels or electro-fuels. Both pathways produce a liquid hydrocarbon fuel, with the former relying on bio derived feedstocks (dedicated energy crops or waste valorisation). Electro-fuels, by comparison, are produced through the synthesis of green hydrogen alongside renewably sourced CO_2, ideally from direct air capture, to produce synthetic SAF. Bio derived feedstocks are limited and compete with food and general land use, and are therefore not considered sustainable in the long term [2]–[4]. For this reason, synthetic SAF is the focus of this study and will be referred to as SAF for the remainder of this paper.

SAF is envisaged to be the main driver of decarbonisation [5], however SAF requires a considerable amount of renewable electricity for its production – Synkero, a start-up company for the production of synthetic kerosene, claim that 30 off-shore wind turbines (1,200 GWh) are required for the production of 1% of all fuel used in Schiphol airport in 2019 [6]. Furthermore, if all 95 billion gallons of jet fuel consumed by commercial airlines globally in 2019 were to be replaced with SAF, it could demand between 244-489% of all wind and solar electricity generated in 2021, based on SAF production efficiencies of 25-50% [7], [8]. The efficiency of sustainable fuel production effectively means that at least two times the amount of fuel energy consumed in aviation must be replaced with renewable electricity – this will place a massive strain on any country's energy resources, in a world where energy is becoming scarce, and energy security is at an all-time low. Therefore, it is critical that the pathway of minimum energy consumption is chosen, where possible.

Uncertainty in fuel choice arises in the different fuel properties of hydrogen and SAF, as well as the varying production efficiencies and costs. Liquid Hydrogen (LH2) can be used directly to fuel aircraft, however LH2 propulsion can require complex cooling systems and large, heavy tanks due to the 4x volume increase of LH2 over SAF. This means that despite its higher specific energy, hydrogen generally results in lower in-flight performance compared to kerosene (or SAF) [9]. SAF yields a lower production efficiency due to the additional processing steps associated with the carbon capture process, but benefits from higher in-flight performance, as well as being a 'drop-in' replacement for kerosene, removing infrastructure and technology barriers associated with hydrogen. Thus, there is a 'break-even' point where flights below a certain range will consume less WtW renewable electricity with direct combustion of LH2, and thus may yield a lower overall cost on a per-seat-kilometer basis in the years 2035 and 2050 [9].

The challenge then becomes the implementation of these alternative fuels. The sector will require green hydrogen resources regardless of the pathway chosen, but the allocation of these green hydrogen resources is unclear. Should the renewably sourced hydrogen be used directly in hydrogen aircraft? Should the hydrogen be allocated towards SAF production to be used in conventional aircraft? Or should it be a combination of both, and if so, there must be some optimum allocation of hydrogen between direct LH2 combustion and SAF production that minimises the renewable electricity demand from the grid. This allocation of green hydrogen must be motivated from an engineering analysis, which optimises green hydrogen use in such a way that an optimum, or minimum energy demand on the grid, is achieved. Hence, this study aims to both quantify and reduce the strain placed on renewable electricity production in the transition to sustainable aviation, and determine the optimum fuel choice for short-haul aviation from a WtW energy perspective. Specific objectives of this study include:

- Sizing of three Boeing 737-800NG hydrogen aircraft to incorporate hydrogen tanks of varying gravimetric efficiencies, maintaining fixed passenger capacity and design range
- Modelling of sample real-world operation schedule of B737-800NG fleet using LH2 and SAF aircraft
- Comparative in-flight and WtW energy analysis of each operation schedule
- Sensitivity analysis based on SAF production efficiencies
- Analysis of renewable electricity requirements for full day of airline operations

III. Methodology

A. Aircraft Model

1. Boeing 737-800NG

A Boeing 737-800NG model was developed within SUAVE, using detailed airframe geometry information obtained from [10]. The built-in propulsion model within SUAVE uses a simplified analytical approach based on the methods of Cantwell [11], and approximates the performance by using a single operating point efficiency, based on the design point efficiency. As a result, the SUAVE propulsion model does not account for off-design efficiency, and thus the TSFC is a function of only the altitude and Mach number. An example of the simplistic propulsion modelling in SUAVE can be seen in the work of Dorsey and Uranga [12], which used fixed stage efficiencies and pressure ratios throughout the propulsion system simulations. Due to the lack of off-design representation within the built-in SUAVE propulsion model, a higher-fidelity model was developed using NASA's Numerical Propulsion System Software (NPSS) [13], further described in Section III.B.

2. Aerodynamics

The aerodynamic model used within SUAVE is known as the 'Fidelity-Zero' model, which is based on the Vortex-Lattice Method (VLM). The VLM is used to calculate the inviscid lift through discretisation of the wing into panels, and calculation of the strength of the trailing vortices and their downwash effect using the Biot-Savart law [14]. Factor based corrections to account for the lift effects of the fuselage, compressibility and viscous effects are applied to the inviscid wing lift to obtain the total aircraft lift [15].

The aircraft drag is comprised of the parasite drag, lift-induced drag, compressibility drag and miscellaneous drag. The parasite drag is the drag associated with skin friction and pressure drag, and is computed for the fuselage, wings and nacelles. The fuselage and wing parasite drag is calculated using Eq. (1), in which the evaluation of the form factor *k* varies for each calculation. The lift-induced drag is composed of viscid and inviscid components. The inviscid lift-induced drag is obtained from the VLM calculation, while the viscid component is calculated using a viscous lift-dependent drag factor [15]. The compressibility and miscellaneous drag is calculated using correlations from Shevell [16] and Kroo [17]. The lift and drag correction factors were calibrated to minimise the error of SUAVE fuel burn predictions with respect to the actual fuel burn for >25 flights contained within the flight database. Further details of this calibration can be obtained from the work of Gallagher et al. [18].

$$C_{D_P} = k \cdot C_f \cdot S_{ref} \tag{1}$$

3. Mission Solver

The SUAVE mission solver works by iterating the unknowns of a mission segment, generally the throttle and pitch angle, until the residuals are converged. In the case of cruise, the residuals are the sum of horizontal and vertical forces, which are converged to zero [15]. For the climb and descent segments, a 'linear speed, constant rate' segment was used, which models an accelerating/decelerating aircraft moving with a constant vertical rate of climb/descent. The cruise segment was modelled using a 'constant speed, constant rate, loiter' segment, which models an aircraft with steady, constant altitude motion for a prescribed length of time.

B. Propulsion Model

1. CFM56-7B26/3

NASA's NPSS was used to develop a surrogate propulsion model of the CFM56-7B26/3 engine to be integrated within the overall SUAVE aircraft model. Inclusion of the NPSS propulsion model enabled accurate off-design propulsion system analysis through the use of component performance maps. The surrogate model was generated using Gaussian process regression methods, which formulates a continuous function for thrust and SFC based on the nearby points of the discrete NPSS dataset, using a normal distribution [19]. NPSS was chosen as the propulsion system software due to the extensive use of the tool throughout published literature for both existing and unconventional designs [20]–[24], along with the presence of documented validations [24]–[26], combined with the

collective experience of contributors NASA and consortium members such as GE Aviation, Boeing, Rolls-Royce, Lockheed Martin and others [27].

Fig. 1 illustrates the CFM56 turbofan model in block diagram form, outlining the various components used within the model. The model was calibrated to match ICAO testbed data for Sea-Level-Static (SLS) operating points, in which the component design variables were used to vary the model outputs. Component design variables include compressor/turbine pressure ratios and stage efficiencies, along with the combustor outlet temperature and bypass ratio. For off-design analysis, generalised component performance maps were used, based on a late 1980's advanced technology turbofan developed by NASA in their energy efficient engine programme [28].

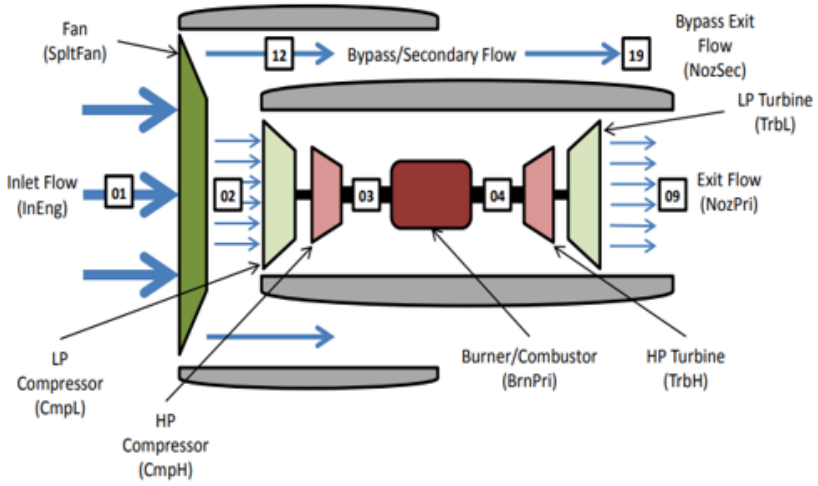

Fig. 1 Block diagram of NPSS CFM56-7B26/3 turbofan model [27]

2. Validation Results

The final validation results of the calibrated turbofan model are presented in Table 1. Validation errors are calculated with respect to the ICAO SLS data, obtained from the ICAO Emissions Databank [29], along with published CFM56-7B SFC values for the top-of-climb and rolling take-off operating points from a NASA numerical study [26]. The exact engine variant modelled by NASA in that publication is unclear, hence there is uncertainty in these reported TSFC figures. The propulsion model had a high level of accuracy, with the TSFC of three out of four SLS points predicted within 1% accuracy of the measured values. The largest TSFC error was obtained for the 30% power point at SLS, with a relative error of -5.71%. This outlier in the validation results may be explained by the use of the generalised component performance maps, as the shape of the speedlines could vary significantly with respect to the actual, proprietary performance maps of the CFM56 turbofan. While this error is relatively insignificant due to the low fuel-flow values at this operating point, further improvements could be obtained through using an optimiser to calibrate the component design variables, and generate scaling coefficients for the component performance maps in order to minimise the validation errors.

Table 1 NPSS validation results for CFM56-7B26/3 turbofan model

Operating Point	Thrust (lbf)	Thermal Eff.	Predicted SFC (lbm/hr.lbf)	NASA/ICAO SFC	Error
Top-of-Climb	5960	54%	0.635	0.650	-2.31%
Rolling-Take-Off	20954	46%	0.473	0.474	-0.21%
SLS – 100% power	26300	46%	0.369	0.366	0.82%
SLS – 85% power	22355	45%	0.352	0.350	0.57%
SLS – 30% power	7890	32%	0.314	0.333	-5.71%
SLS – 7% power	1841	15%	0.464	0.466	-0.43%

Following the validation, a hydrogen powered model of the CFM56-7B26/3 turbofan was developed by switching the fuel used from kerosene to hydrogen. Hence, it was assumed that no engine modifications are required for hydrogen powered operations, i.e. the fuel flow rate is a function of the lower heating value only, which was a simplification in this analysis.

C. Hydrogen Aircraft Sizing

Following the development of the baseline model, three hydrogen powered B737-800NG aircraft were sized to facilitate incorporation of fuel tanks with varying gravimetric efficiencies. The aircraft were sized for the baseline design mission, with a design range of 2950 NM and a payload of approximately 20 tonnes.

1. Tank Design

The liquid hydrogen tank design was sized using the required fuel along with the gravimetric efficiency, which is defined in Eq. (2). The general design parameters, such as insulation and tank wall thickness, were based on the values provided by Huete et al. [30] for short/medium-haul applications, based on their parametric analyses of tank designs. This tank was designed for a dormancy time of 24 hours – i.e. venting of hydrogen gas is required after 24 hours, to prevent the tank operating pressure breaching its maximum limit of 404 kPa following hydrogen boil-off. The useful LH2 capacity of this tank was approximately 6000 kg, which is within the range of fuel mass used within this study. The gravimetric efficiency for this tank design was 66%, which is an optimistic, but achievable value according to the detailed analysis provided by Huete et al. [30]. To account for uncertainties in tank gravimetric efficiencies, three values of 33%, 50%, and 66% were utilised in this study. The design parameters for the final tank design are outlined in Table 2.

$$\eta_{grav} = \frac{m_{fuel}}{m_{fuel} + m_{tank}} \tag{2}$$

Table 2 Design parameters for liquid hydrogen tank [30]

Dormancy	Diameter	Insulation Thickness	Wall Thickness	Gravimetric Efficiencies
24 hrs	3.6 m	310 mm	3.27 mm	33%, 50%, 66%

2. Sizing Loop

A sizing loop was developed to generate the hydrogen aircraft designs. Using an initial hydrogen fuel mass estimate based on the equivalent energy of the baseline kerosene aircraft fuel mass, a hydrogen tank was designed to be housed within an extended fuselage, where the length of the new fuselage was extended by the length of the hydrogen tank. The wings and engine were re-sized, maintaining constant wing loading and thrust-to-MTOW ratios. The weight of the new fuselage and wings were estimated using the weight estimation methods contained within SUAVE [15], while the weight of the engines were scaled linearly in proportion with the new design thrust. Scaling of the horizontal and vertical tail components was ignored in the current analysis, as these components primarily affect stability and would have a minimal effect on the fuel-flow performance. Stability analysis was outside the scope of this study. Convergence of the aircraft design was achieved when the difference in MTOW between iterations was <0.001%. Fig. 2 illustrates the sizing process described above, where *i* refers to the iteration count.

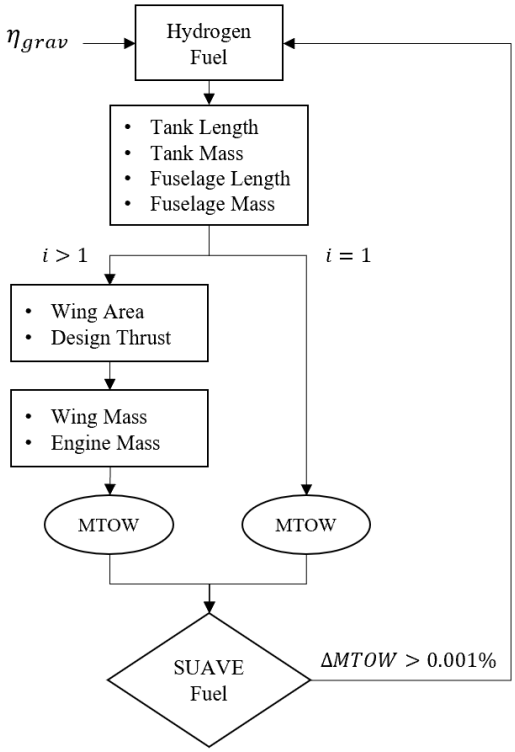

Fig. 2 Sizing process for hydrogen aircraft

3. Final Aircraft Designs

The final aircraft designs are presented in Table 3. The SAF aircraft is equivalent to the conventional Boeing 737-800NG aircraft used to collect the data from the flight database. The three LH2 designs differ by tank gravimetric efficiency, where the efficiencies equal 33%, 50%, and 66%. The significance of this parameter can be seen through the exponential effect on aircraft weight and fuel burn – as seen from the results in Table 3, and illustrated in the component mass graph in Fig. 3. This is due to the compounding effect of the tank efficiency; lower gravimetric efficiency resulted in a larger tank weight, which increased the fuel required, increasing the fuselage length and weight further, which then required larger wings and engines to maintain sufficient lift and thrust. R_{fuel} in Eq. (3) is the ratio of design mission fuel burn relative to the SAF configuration, which is used in the take-off weight estimation method for the hydrogen aircraft missions, as outlined in Section D.3.

$$R_{Fuel} = \frac{m_{fuel}}{m_{fuel,SAF}} \tag{3}$$

Table 3 Sizing results for B737-800NG hydrogen aircraft

Configuration	Fuel Mass (kg)	Tank Mass (kg)	Fuselage Length (m)	MTOW (kg)	R_{fuel}
SAF	17738.7	---	38.02	79016	1.0
LH2-33	11446.9	23240.8	59.95	116076	0.645
LH2-50	7521.7	7521.7	51.96	82935	0.424
LH2-66	6858.5	3533.2	50.61	76144	0.387

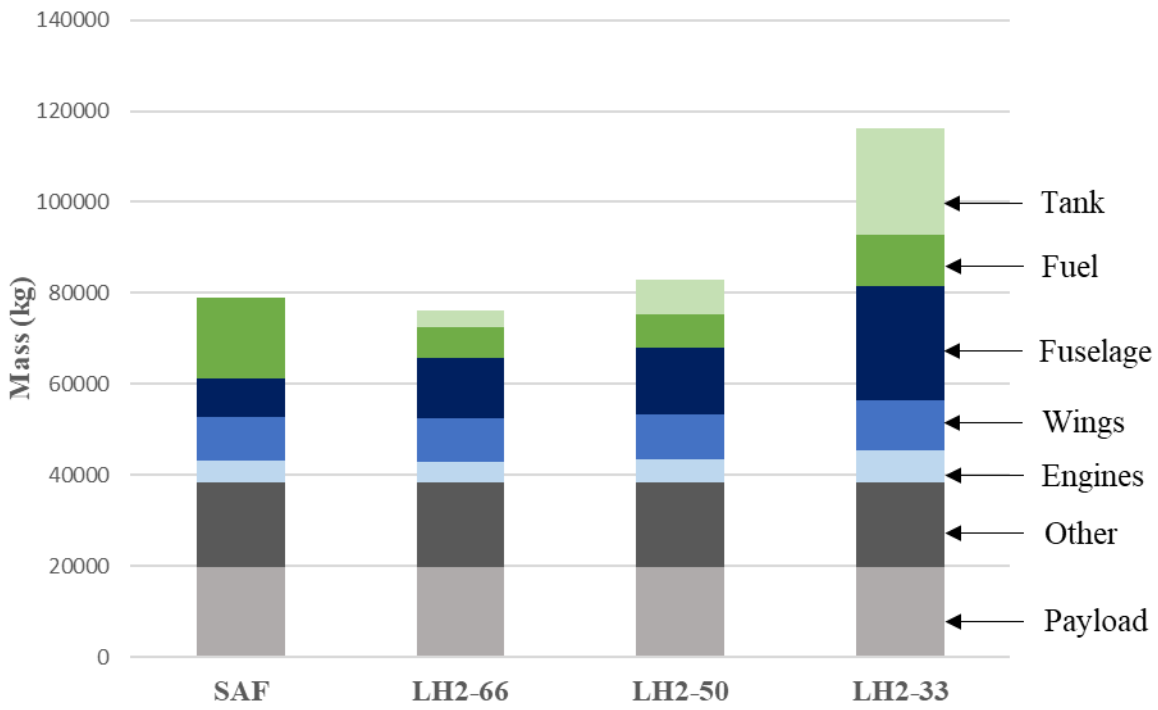

Fig. 3 Component mass distribution of SAF and hydrogen aircraft

D. Real-World Operations

1. Flight Database

The flight database contains crucial flight information from an airline, such as take-off weights and average fuel-flow per flight segment, for 29 flights of B737-800NG aircraft over two days. This flight database enabled the validation and calibration of the current aircraft model, as detailed in the work of Gallagher et al. [18]. Furthermore, this flight database enabled the current analysis of real-world operations with potential future aircraft, projecting the anticipated energy demand, and hence the anticipated cost, of future operations for an airline. The distribution of the sample flights is presented in Fig. 4 in terms of flight range and TOW, where TOW values have been redacted due to the sensitive nature of the data.

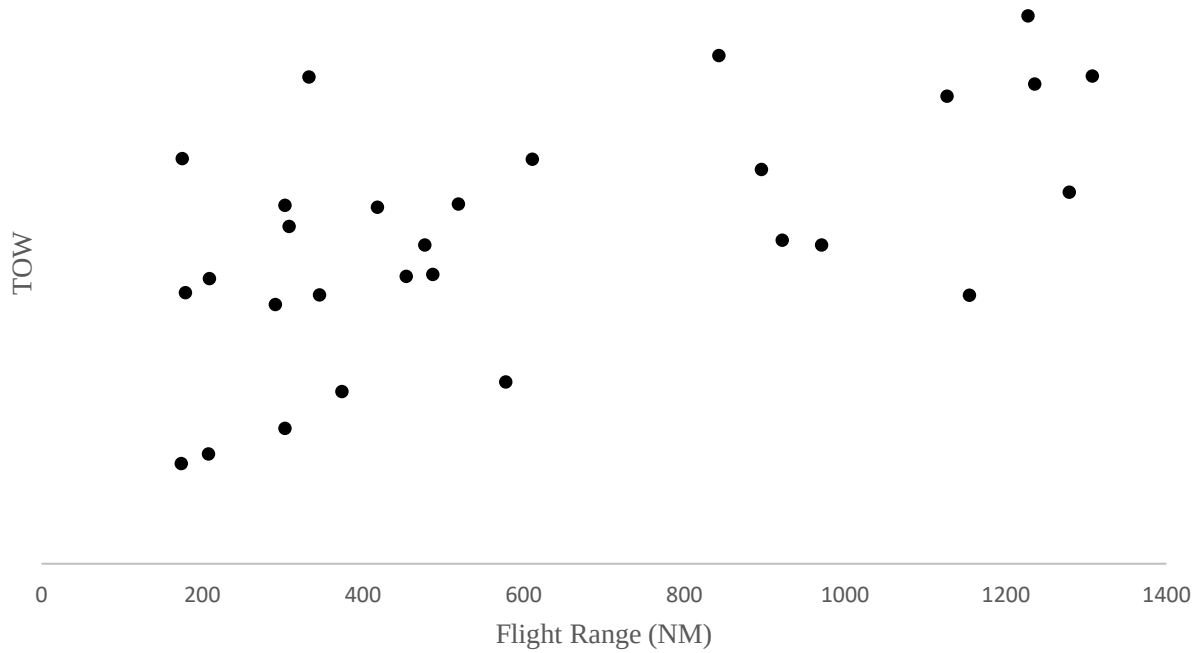

Fig. 4 Distribution of B737-800NG missions from available flight database in terms of range and TOW

2. Flight Paths

Real flight paths were obtained from Automatic Dependent Surveillance-Broadcast (ADS-B) data to ensure the simulations were representative of real-world conditions. Publicly available timestamped coordinates were downloaded, from which the flight path details in terms of the altitude and speed were calculated using MATLAB. The flight path was approximated using linear piece-wise segments, outlining information such as the initial and terminal altitude, initial and terminal speed, and the rate of climb/descent to be input to SUAVE for each segment.

The climb and descent segments each consisted of 18 linear sub-segments to ensure an accurate representation of the flight paths. Cruise was approximated using a single, level, linear segment with a constant speed and constant altitude, ignoring any step-climb/descent operations. The initial climb, approach, and final approach sub-segments, which are separated from climb and descent due to the deployment of flaps/slats and landing gear, were each represented by a single sub-segment using the same parameters as climb and descent. It is important to note that the true airspeed profile was unavailable for these flights, hence the effect of wind speed is unaccounted for in the current analysis. An example of this flight path approximation for a mission from the flight database is presented in Fig. 5.

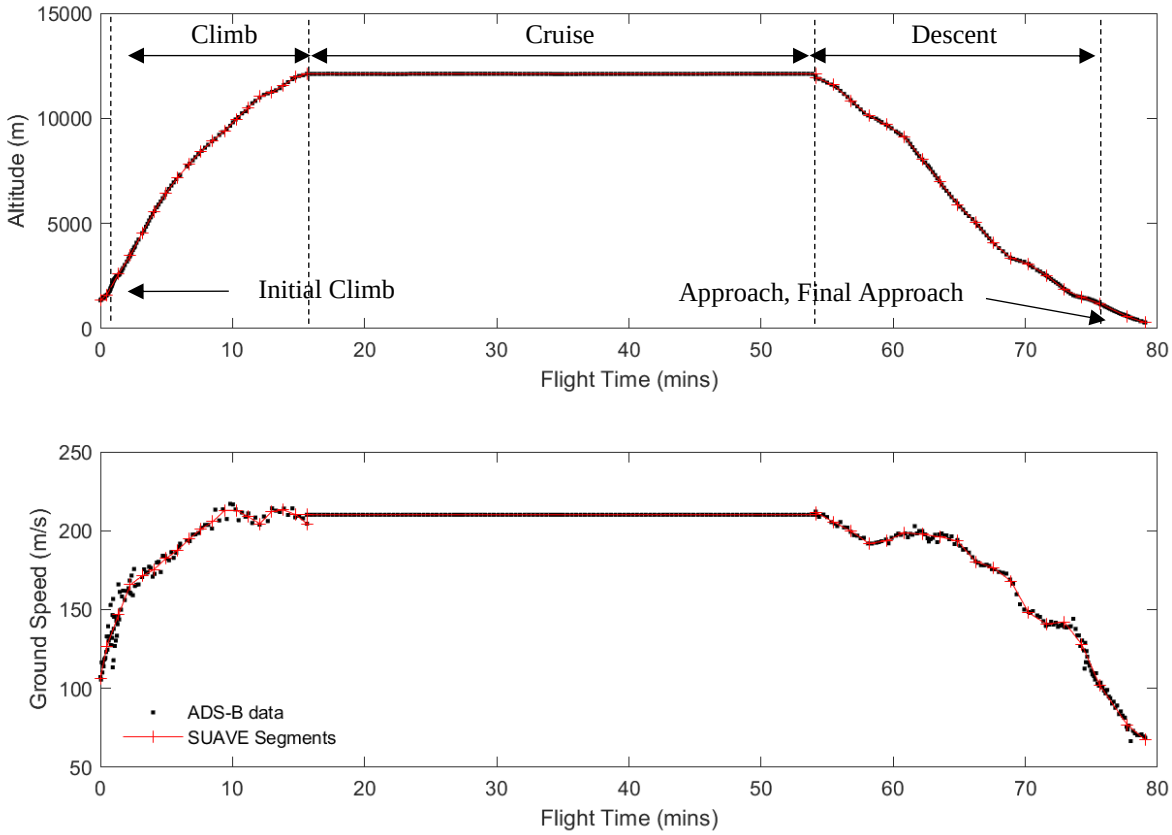

Fig. 5 Flight path altitude and speed approximation for SUAVE input

3. Hydrogen Take-off Weights

While the take-off weights for the real-world kerosene (SAF) aircraft missions were provided through the flight database, the take-off weights for the equivalent hydrogen-powered missions had to be estimated. This was done through estimation of the on-board hydrogen fuel carried for each real-world mission. This fuel mass estimation was calculated based on the ratio of design mission fuel burn between the conventional and hydrogen aircraft, labelled R_{fuel} in Table 3 and defined in Eq. (3). This fuel ratio was substituted into Eq. (4) to complete the hydrogen TOW calculation for each real-world mission from the flight database.

$$TOW_{LH_2} = TOW_{SAF} + m_{fuel,SAF}\left(R_{fuel} - 1\right) + m_{tank} + \Delta m_{fuselage} + \Delta m_{wings} + \Delta m_{engines} \tag{4}$$

Where TOW_{SAF} is the actual mission TOW from the flight database, $m_{fuel,SAF}$ is the actual fuel carried onboard for the mission, R_{fuel} is the design mission fuel-ratio from Table 3, m_{tank} is the mass of the hydrogen tank, while $\Delta m_{fuselage}$, Δm_{wings}, and $\Delta m_{engines}$ are the change in fuselage, wing and engine mass between the baseline and hydrogen aircraft, respectively. While this estimate of the hydrogen fuel mass was a simplification, ignoring the variation of in-flight performance at ranges shorter than the design mission, it implicitly captured the magnitude of the reserve fuel carried onboard, as it is based on the actual fuel mass carried onboard for each mission. Furthermore, variations in the onboard fuel mass are less significant for hydrogen due to the high specific energy of the fuel.

E. Sustainable Fuels – Green Hydrogen & Synthetic SAF

The two sustainable fuel choices used in this study are green LH2 and SAF. Both of these fuels require 100% renewable electricity for their production, eliminating carbon emissions. Green hydrogen is produced through electrolysis of water, while SAF is produced through the Fischer-Tropsch process – synthesising green hydrogen with carbon captured from the atmosphere, using a process known as direct air capture. While both of these fuels are

essentially equally sustainable from the perspective of carbon emissions (when produced with 100% renewable electricity), the energy required for their production can vary significantly. The production of green liquid hydrogen yields an efficiency of between 56-58% [9], [31], while the production efficiency of SAF is reported to be between 22-46% [9], [31]. To account for the uncertainty in synthetic SAF production efficiency, this study utilised three SAF production values – pessimistic, baseline, and optimistic, while a constant efficiency of 57% was used for green liquid hydrogen, as outlined in Table 4.

Table 4 Production efficiencies used for green liquid hydrogen and synthetic SAF

Fuel Type	Pessimistic	Baseline	Optimistic
Green LH2	57%	57%	57%
SAF	22%	34%	46%

IV. Energy Analysis

A. In-Flight Energy Performance

For each aircraft design, the missions from the flight database outlined in Section III.D were modelled in SUAVE, and the fuel burn was recorded. Three sample missions were selected for detailed analysis, comprising of a short, medium and long-range mission in the context of the available database, which are presented below.

1. Short-Range (200 NM)

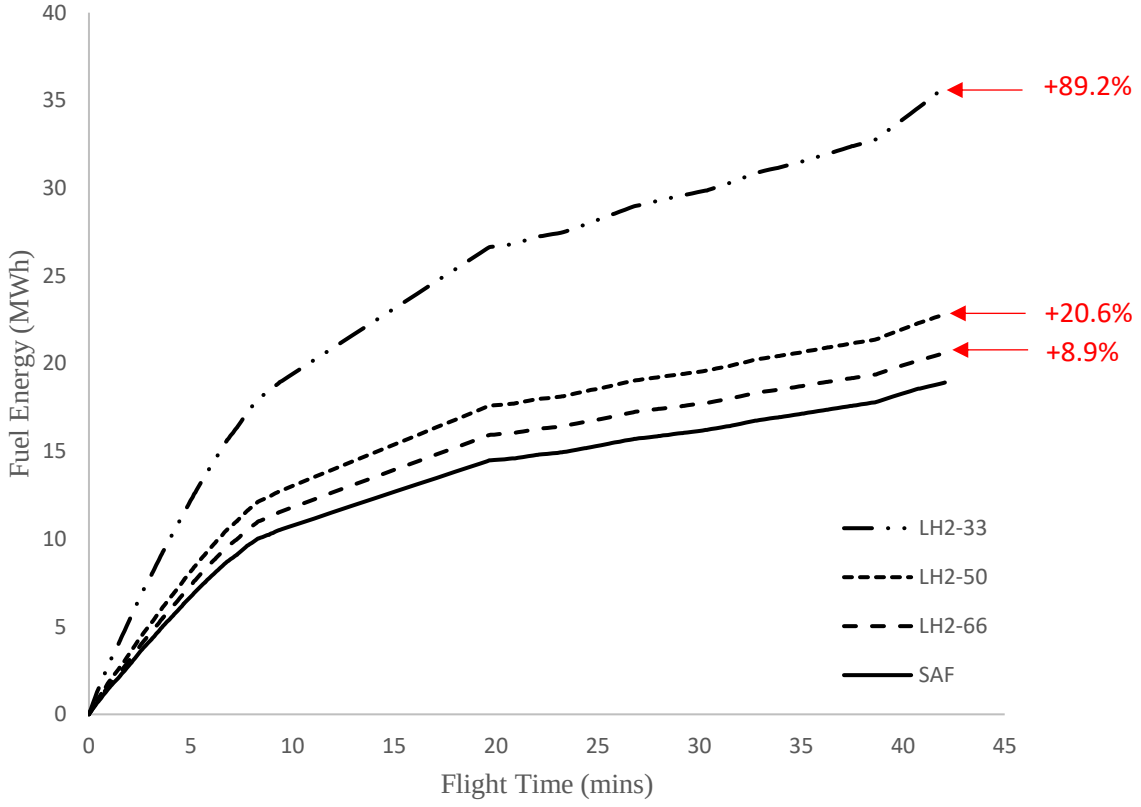

Fig. 6 In-flight energy consumption for hydrogen and SAF aircraft on 200 NM mission

Figure 6 shows the in-flight energy performance of each aircraft on a 200 NM mission. As expected, the SAF aircraft yielded optimum in-flight performance, followed by the LH2-66, LH2-50, and LH2-33 configurations. The LH2-33 candidate performed significantly worse than all other aircraft, consuming 89.2% more energy than the SAF aircraft. Note the increased slope of energy consumption during the climb and final approach segments at the

beginning and end of the flight – the LH2-33 aircraft suffered large performance penalties during these climb and landing phases due to the high dependency on lift-induced drag during these segments. As the LH2-33 configuration was significantly heavier than the other aircraft, it experienced much larger drag, resulting in an increased rate of fuel consumption. The LH2-50 and LH2-66 configurations had much lower take-off weights (30.6% and 37% lower, respectively), hence the lift-induced drag, and thus the rate of energy consumption, was more comparable with the SAF aircraft. The LH2-50 and LH2-66 configurations suffered energy performance penalties of 20.6% and 8.9%, respectively.

2. Medium-Range (900 NM)

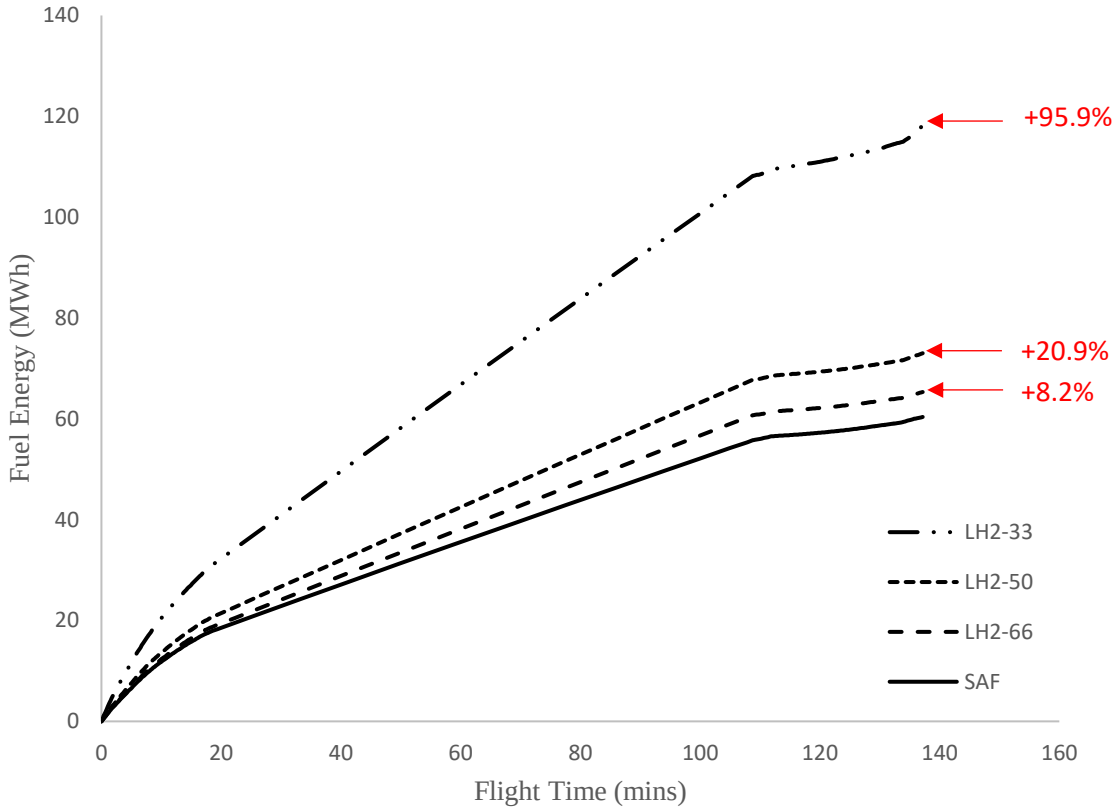

Fig. 7 In-flight energy consumption for hydrogen and SAF aircraft on 900 NM mission

Fig. 7 shows the in-flight energy consumption of each aircraft on the medium-range 900 NM mission. The trends in performance are largely consistent with the short-range mission, as the SAF aircraft out-performed all hydrogen aircraft, whereas the LH2-33 aircraft displayed significantly worse performance than all other aircraft candidates. Some interesting trends did appear, however. The LH2-33 configuration suffered from greater performance penalties with increased mission range, as the energy consumption increase relative to SAF increased from 89.2% to 95.9%. The LH2-50 configuration experienced a minor increase in performance penalties, as the energy consumption relative to SAF increased from 20.6% to 20.9%. Most notably, the energy increase of the LH2-66 configuration relative to SAF reduced from 8.9% to 8.2%. With the increased operating empty weight and additional fuselage drag of the hydrogen aircraft, it would be expected that increased mission range would further exacerbate the in-flight performance penalties.

3. Long-Range (1300 NM)

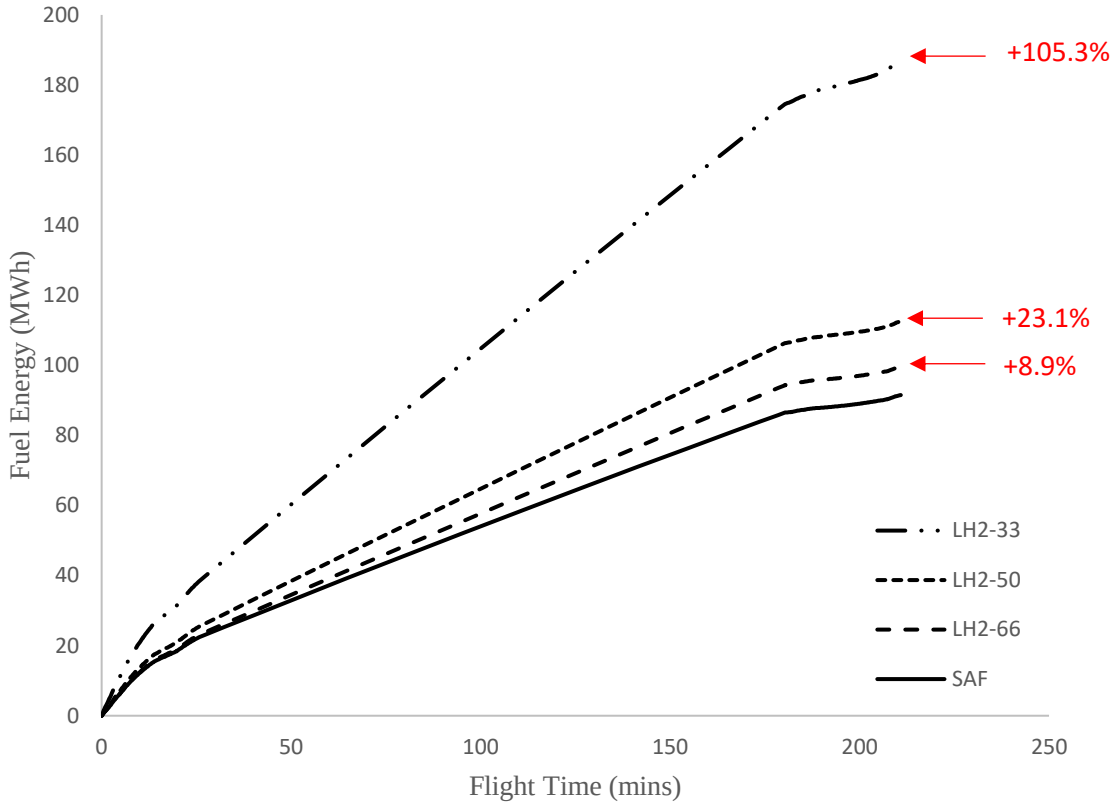

Fig. 8 In-flight energy consumption for hydrogen and SAF aircraft on 1300 NM mission

The in-flight energy consumption results for the longest flight within the flight database are presented in Fig. 8. The trends discussed in the previous sections were continued here, as the in-flight performance penalties increased for each of the hydrogen aircraft configurations. The relative increase in performance penalties between the 900 and 1300 NM missions for the LH2-33 and LH2-50 configurations (95.9% → 105.3% and 20.9% → 23.1%) were similar or greater than the relative increase in performance penalties between the 200 and 900 NM missions (89.2% → 95.9% and 20.6% → 20.9%) despite a 300 NM difference in range increase (900 → 1300 and 200 → 900), which suggests that the greater the increase in mission range, the greater the increase in relative performance penalties. This suggests a non-linear effect on energy performance with respect to mission range, which could be due to the large increase in operating empty weight carried throughout the increased mission distance, and the reduced effect of weight reduction due to fuel burn throughout the mission compared to the SAF aircraft.

Observing the LH2-66 results from the short, medium and long-range missions, it would appear that an optimum mission range exists between 200 and 1300 NM for the LH2-66 configuration. A potential explanation for this is the nature of the real-world operations modelling, which modelled all aircraft on the same flight path, with varying quantities of on-board reserve fuel for each real-world mission (based on the airline's turnaround/re-fueling strategy). This flight path would have been optimised for the given aircraft on the day, i.e. the SAF aircraft, however it was likely sub-optimal for different aircraft with different take-off weights. For instance, the SAF aircraft flew at a specified cruise altitude and speed such that the required Angle of Attack (AoA) led to an optimum, i.e. maximum, Lift to Drag (L/D) ratio. A change in the hydrogen aircraft TOW meant that for the same cruise altitude and speed, a change in AoA was required within he model, leading to a change in the L/D ratio, which affected the hydrogen aircraft performance. Similarly, steeper climb angles during the climb segment would yield a greater impact on the performance of heavier hydrogen aircraft, due to the increased effect of lift-induced drag. Furthermore, each real flight mission carried different quantities of reserve fuel, resulting in fluctuating performance effects between the modelled SAF and hydrogen aircraft missions across the different flights. Real missions with larger quantities of reserve fuel would benefit the hydrogen missions, whereas those with lower quantities would have a negative impact on the hydrogen missions compared to the SAF missions, due to the higher specific energy of hydrogen versus SAF.

4. Fleet-Wide In-Flight Energy Performance

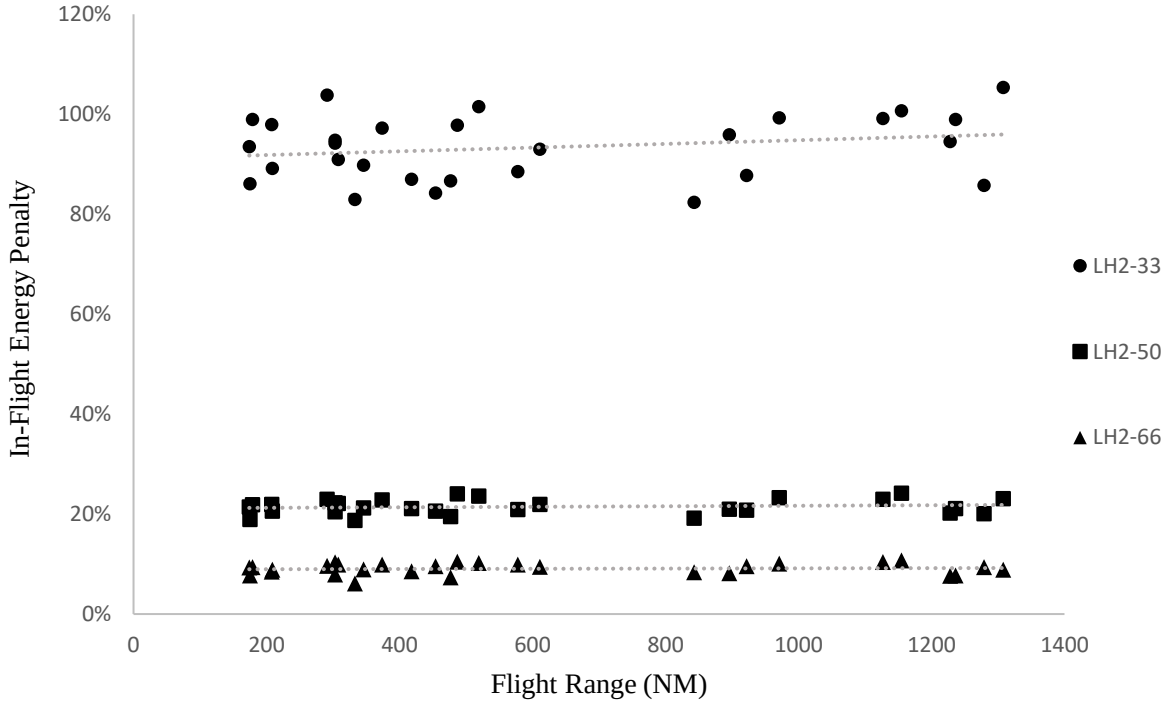

Fig. 9 Fleet-wide in-flight energy performance penalties of hydrogen aircraft vs. SAF aircraft

Fig. 9 illustrates the in-flight energy performance penalties for the three hydrogen configurations compared to the SAF aircraft. The results in the previous section indicated that there may be a non-linear trend of increased energy performance penalties with respect to flight range, however the results in Fig. 9 show that this is not the case. For the LH2-33 configuration, there is a notable linearly increasing trend of performance penalties with respect to flight range, while for the LH2-50 and LH2-66 configurations, there is a slight, but visible linear trend of increased performance penalties with range.

The fluctuating energy performance penalties observed across the various missions can be explained through the reasoning provided in the previous section, in which the nature of the real-world operations model imposed a varying effect on the energy penalties across the different missions. To further reinforce this point, the LH2-33 missions with the lowest in-flight energy penalties (80-85%) were compared to those with the highest performance penalties (100-105%). It was found that the lower performance penalties were associated with a lower hydrogen aircraft TOW relative to the SAF TOW, which benefitted these hydrogen missions through a higher L/D ratio. In addition, a higher reserve fuel quantity was carried on-board for the missions exhibiting a reduced performance penalty (up to 9.4% of the TOW in mass), leading to greater relative mass savings for the hydrogen aircraft compared to the equivalent SAF missions.

B. Well-to-Wake Energy Performance

The previous section analysed the in-flight energy performance of each configuration, however, in the context of decarbonisation, the production energy of each respective fuel must be considered. Generally, a larger WtW energy consumption indicates a higher end-cost – particularly during periods where energy costs are high. This was highlighted in the study by Zhou et al. [32], where synthetic SAF costs in the EU were projected to be higher than the US due to the increased price of renewable electricity. Three fuel production efficiency values were utilised for the single SAF aircraft with values of 22%, 34%, and 46% (labelled SAF-22% etc.), while liquified hydrogen production was set at a constant efficiency of 57%. Note that the LH2-33, LH2-50, and LH2-66 configurations refer to hydrogen aircraft designed with tank gravimetric efficiencies of 33%, 50%, and 66%, respectively.

1. Short-Range (200 NM)

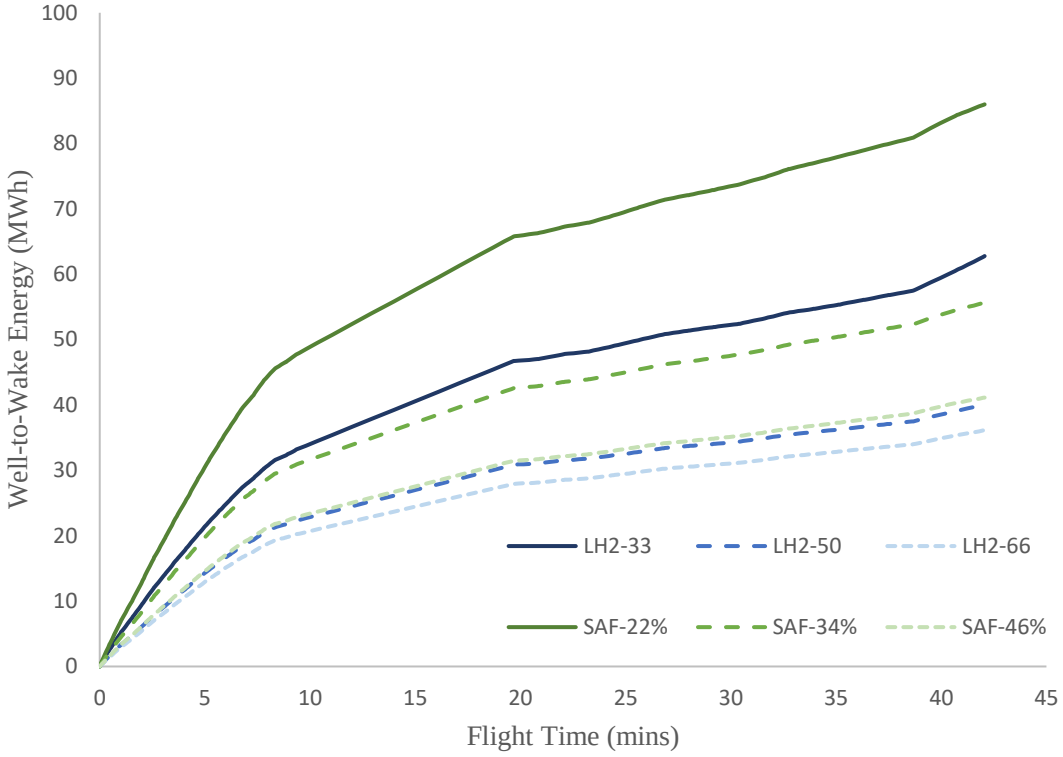

Fig. 10 Well-to-Wake energy consumption for hydrogen and SAF aircraft on 200 NM mission

Fig. 10 shows the WtW energy consumption for the short-range mission. The pessimistic SAF scenario, i.e. SAF-22%, consumed significantly more energy than all other configurations, in which it required 37% more energy than the LH2-33 aircraft, despite the large in-flight performance penalties experienced by the LH2-33 aircraft. Even for the baseline SAF scenario, i.e. SAF-34%, a moderate energy saving of only 11.4% was observed compared to the LH2-33 candidate. The LH2-66 aircraft consumed the least energy, followed by the LH2-50 aircraft, however the optimistic SAF scenario, SAF-46%, showed comparable performance.

2. Medium-Range (900 NM)

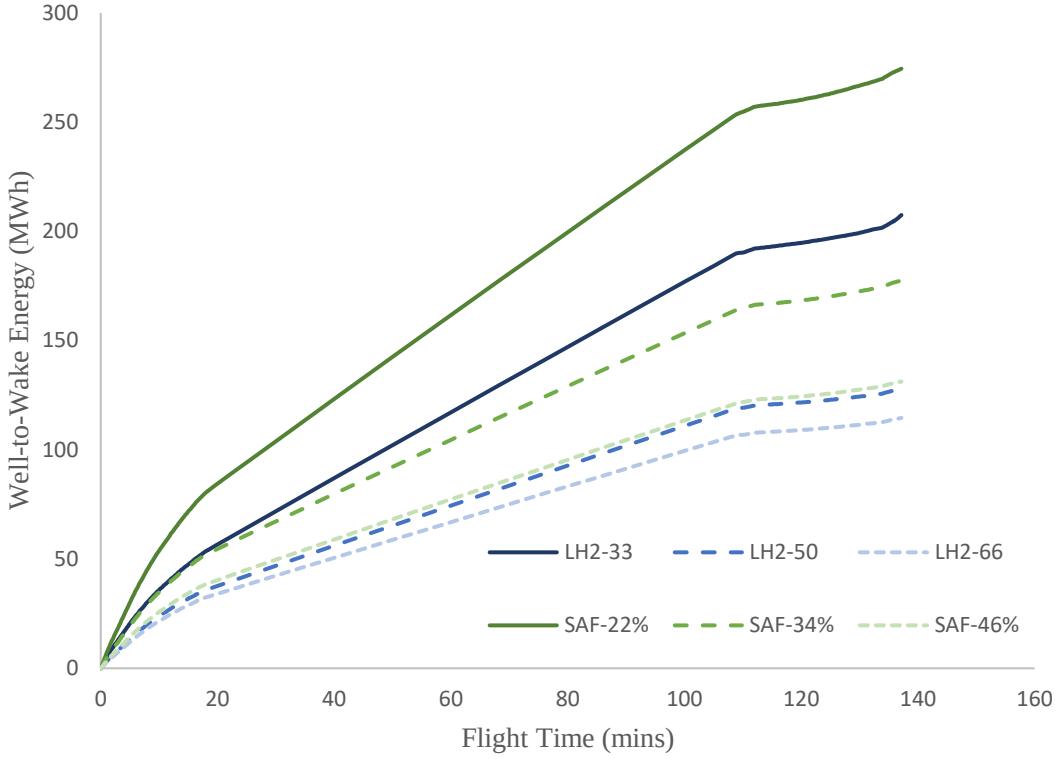

Fig. 11 Well-to-Wake energy consumption for hydrogen and SAF aircraft on 900 NM mission

Fig. 11 shows the WtW energy consumption for the medium-range mission, where similar trends were observed compared to the short-range mission. The energy penalty for the SAF-22% scenario relative to the LH2-33 aircraft decreased from 37% to 32.3%, whereas the energy savings of the SAF-34% scenario relative to the LH2-33 aircraft increased from 11.4% to 14.4%. Again, the LH2-66 aircraft yielded optimum performance, followed by the LH2-50 aircraft, which performed similarly to the optimistic SAF-46% scenario.

3. Long-Range (1300 NM)

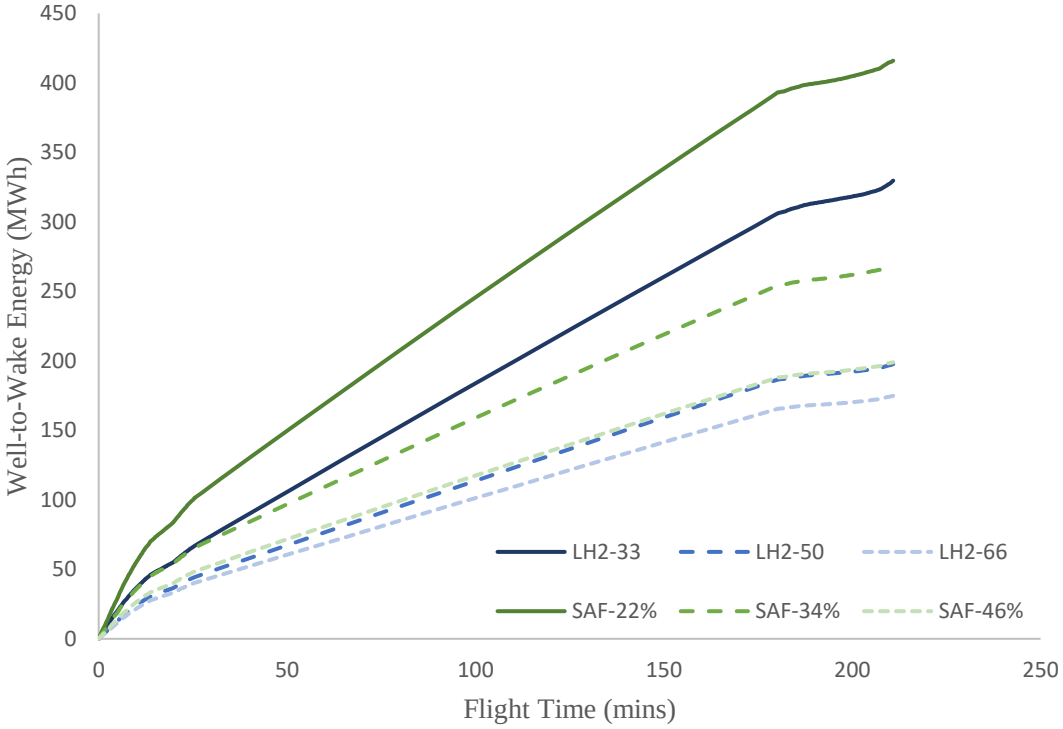

Figure 12 Well-to-Wake energy consumption for hydrogen and SAF aircraft on 1300 NM mission

Fig. 12 shows the WtW energy consumption for the long-range mission, where the energy penalties of the SAF-22% scenario relative to the LH2-33 aircraft reduced to 26.2%, whereas the energy savings of the SAF-34% scenario relative to the LH2-33 aircraft increased to 18.4%. The LH2-66 aircraft maintained optimum performance, while the LH2-50 aircraft achieved parity with the optimistic SAF-46% scenario.

4. Fleet-Wide Well-to-Wake Energy

Table 5 Well-to-Wake energy consumption of LH2 and SAF scenarios (29 flights)

Configuration	Total Fuel Energy (MWh)	Prod. Efficiency	WtW Energy (MWh)
SAF-22%	1248.3	22%	5674.2
SAF-34%	1248.3	34%	3671.6
SAF-46%	1248.3	46%	2713.8
LH2-33	2422.4	57%	4249.9
LH2-50	1517.3	57%	2661.9
LH2-66	1361.7	57%	2388.9

Table 5 shows the total fleet-wide fuel energy for each configuration, and the associated WtW energy consumption. The significance of the production efficiency was observed through comparison of the SAF-22% and LH2-33 WtW energy consumption, which equal 5.67 GWh and 4.25 GWh, respectively. Despite the substantially larger in-flight energy consumption of the LH2-33 aircraft compared to the SAF aircraft, a SAF production efficiency of 22% completely eliminated any potential energy savings. In fact, the pessimistic SAF production efficiency resulted in an overall energy penalty of 33.5% when compared to the LH2-33 aircraft. More optimistic SAF production efficiencies of 34% and 46% were sufficient for energy savings against the LH2-33 configuration, however, the LH2-50 and LH2-66 aircraft out-performed all SAF scenarios in terms of WtW energy consumption. The SAF scenarios resulted in energy penalties between 1.9% and 113.2% when compared to the LH2-50 aircraft, whereas energy penalties between

13.6% and 137.5% were obtained for the SAF scenarios when compared to the energy consumption of the LH2-66 aircraft. The baseline configuration for each fuel, i.e. SAF-34% and LH2-50, resulted in a WtW energy increase of 37.9% for the SAF aircraft relative to the LH2 fueled candidate.

The substantial effect of both SAF production efficiencies and hydrogen tank gravimetric efficiencies on the total energy consumption was observed in this analysis. It can be concluded that a gravimetric efficiency of 50% is sufficient for comparable, or improved energy performance against all SAF scenarios. Furthermore, it could be suggested that a SAF production efficiency of at least 46% is required to maintain acceptable WtW energy performance for SAF aircraft against their hydrogen counterparts – as the magnitude of energy penalties for the SAF-22% and SAF-34% scenarios would be unsustainable in the long-term to decarbonise the entire aviation industry.

C. Renewable Electricity

The previous section calculated the total WtW energy consumption for each of the LH2 and SAF scenarios, which is equivalent to the renewable electricity demand required for the fuel production of each scenario. Ultimately, the projected cost of these sustainable fuels are uncertain, requiring detailed models accounting for factors such as the fuel production capital costs, the assumed efficiencies of each process, and projected carbon costs [32]. However, the projected cost of renewable electricity production is easily obtained and does not require a new model for the different fuel production efficiencies. Therefore, this analysis considers the magnitude and cost of the renewable electricity for the production of each sustainable fuel scenario, which estimates the scale of renewable electricity investment required and provides a conservative indication of the final fuel costs in each scenario.

Due to the significant scale of renewable electricity required, it is likely that off-shore wind will provide the majority of renewable electricity for such applications in Europe towards 2050. Projects such as the North Sea (NS) wind power hub have pledged to install 120 GW of off-shore wind capacity by 2030, rising to 300 GW by 2050 to become "Europe's biggest green power plant" [33]. For this reason, off-shore wind was selected as the basis for this analysis, which investigates the total renewable electricity demand as a percentage of the total 2050 projected NS energy production (4.11 TWh/day based on a NS wind hub reference study [34]), and the estimated cost of this renewable electricity demand. Furthermore, to enhance the relevance of this analysis, the 29 flights modelled in this study were scaled to a full day of operations for the airline, which were estimated at 3000 flights [35]. Hence, it was assumed that the 29 flights were a representative sample of daily operations, which was a simplification in this analysis.

To estimate the cost of renewable electricity for each scenario, the Levelised Cost Of Electricity (LCOE) for renewable energy was applied to the WtW energy consumption. The LCOE represents the plant-level unit costs for the production of electricity, i.e. the unit cost that electricity should be sold at in order to break-even [36]. The LCOE therefore neglects the mark-up of the electricity sale price, but includes the associated grid connection costs. The LCOE for off-shore wind in the NS beyond 2030 was projected to be an average of €40/MWh [34]. Table 6 shows the LCOE for the 3000 flights in each LH2 and SAF scenario, alongside the proportion of daily renewable electricity production projected for the 300 GW NS off-shore wind hub in 2050. For reference, the equivalent cost of Jet-A fuel, using 2050 EU projected values and carbon tax of $400 per tonne obtained from [9], was €21.46 M.

Table 6 LCOE and proportion of 2050 NS daily energy production of LH2 and SAF scenarios (3000 flights)

Configuration	Renewable Electricity (TWh)	LCOE	NS Daily Production %
SAF-22%	0.5870	€23.48 M	14.3%
SAF-34%	0.3798	€15.19 M	9.2%
SAF-46%	0.2807	€11.23 M	6.8%
LH2-33	0.4396	€17.59 M	10.7%
LH2-50	0.2754	€11.01 M	6.7%
LH2-66	0.2471	€9.89 M	6.0%

The monumental scale of renewable electricity investment required is observed in the results of Table 6. For the pessimistic SAF production scenario, the LCOE was €23.5 M, while the renewable electricity demand was almost 0.6 TWh, which accounts for an estimated 14.3% of the total projected daily electricity generation of the NS wind power hub in 2050. By comparison, the most pessimistic hydrogen aircraft design, i.e. LH2-33, resulted in an LCOE of €17.6 M, consuming 10.7% of the projected NS wind power production. The baseline SAF-34% scenario and LH2-50 aircraft electricity cost was €15.2 M and €11 M, accompanied by a 9.2% and 6.7% utilisation of the projected NS power supplies, respectively. The optimistic SAF-46% scenario and LH2-66 aircraft resulted in an LCOE of €11.2 M

and €9.9 M with power utilisation values of 6.8% and 6%, respectively. Again, this highlights the need for high SAF production efficiencies, or a transition to hydrogen powered aviation on the pathway to net-zero, in order to minimise the enormous strain placed on renewable electricity resources.

While only the SAF-22% scenario resulted in an LCOE value greater than the equivalent projected Jet-A fuel price of €21.5 M, it must be noted that the LCOE only accounts for the price of electricity, and ignores the associated fuel production costs. Furthermore, it must also be noted that the end fuel cost for SAF relative to the LCOE would be much greater than that of hydrogen, as the production of SAF requires production of hydrogen on top of several additional processes (e.g. direct air capture, Fischer-Tropsch) to form the hydrocarbon fuel. However, the LH2-50 and LH2-66 aircraft present a realistic opportunity to reduce operating costs compared to SAF and Jet-A fuel due to the low LCOE values, and the reduced processing steps in the production of hydrogen fuel compared to SAF. Further investigation into the fuel production costs associated for each scenario must be considered in future work.

V.Conclusions

This study performed an energy analysis of real-world B737-800NG short-haul fleet operations using green liquid hydrogen and synthetic SAF, where energy performance was analysed in the context of in-flight energy consumption, and well-to-wake energy consumption. An aircraft model of the B737-800NG aircraft was developed within SUAVE, and a propulsion model of the CFM56-7B26/3 turbofan was developed using NPSS and validated against ICAO data, and connected to the SUAVE tool via a surrogate model.

Three hydrogen aircraft were sized, incorporating liquid hydrogen tanks of various technology levels into an extended fuselage to maintain consistent passenger capacity and design range. The tank gravimetric efficiency had a significant effect on the aircraft size and take-off weights, which contributed to substantial in-flight energy performance penalties for the LH2-33 configuration. Increased gravimetric efficiencies of the LH2-50 and LH2-66 aircraft resulted in significantly improved in-flight energy performance compared to the LH2-33 configuration, however the SAF aircraft yielded optimum in-flight energy performance for all flights within the database.

The WtW energy consumption was obtained for each of the hydrogen aircraft using a constant production efficiency of 57% for the liquid hydrogen. Three SAF production efficiency scenarios were analysed, ranging from a pessimistic value of 22%, to an optimistic value of 46%. It was found that the SAF-22% scenario consumed significantly more energy than all other configurations across a range of missions from 200 – 1300 NM, whereas the SAF-34% scenario obtained moderate energy savings compared to the LH2-33 configuration. The LH2-66 configuration yielded optimum performance in terms of WtW energy consumption, followed by the LH2-50 aircraft, which showed similar performance to the most optimistic SAF scenario. The WtW energy for the 29 flights was scaled to a full day of the airline's operations, estimated at 3000 flights, and the total energy consumption was analysed in the context of the 2050 EU NS wind power hub, in terms of the LCOE and daily power utilisation. The results highlighted the colossal scale of renewable electricity required for decarbonisation, and quantified the potential energy savings with hydrogen powered operations, in which the baseline SAF-34% scenario resulted in an LCOE of €15.2 M and a power utilisation of 9.2%, whereas the hydrogen baseline, LH2-50, resulted in an LCOE of €11 M with a power utilisation of 6.7%.

Therefore, despite the significant in-flight performance penalties, hydrogen aircraft generally performed better than SAF aircraft in terms of the total energy consumption for short-haul operations. Although this was dependent on the liquid hydrogen tank technology level, and the SAF production efficiency, it was found that a tank gravimetric efficiency of 50% was sufficient for increased performance against all SAF scenarios. However, this work examined fleet operations using 2005 aircraft technology levels, future work must consider how the trends develop through the transition to more fuel-efficient aircraft with advanced technologies, alongside a cost-benefit analysis accounting for the significant infrastructural developments required for hydrogen aircraft operations.

Acknowledgments

The authors would like to thank Ryanair for the financial and technical support of this study through the Sustainable Aviation Research Centre at Trinity College Dublin, along with the permission to use their data.

References

[1] A. R. Gnadt, R. L. Speth, J. S. Sabnis, and S. R. H. Barrett, "Technical and environmental assessment of all-electric 180-passenger commercial aircraft," *Progress in Aerospace Sciences*, vol. 105, pp. 1–30, Feb. 2019, doi: 10.1016/j.paerosci.2018.11.002.

[2] "Sustainable biomass availability in the EU, to 2050," *Concawe*. https://www.concawe.eu/publication/sustainable-biomass-availability-in-the-eu-to-2050/ (accessed Nov. 10, 2022).

[3] E. Cabrera and J. M. Melo de Sousa, “Use of Sustainable Fuels in Aviation—A Review,” *Energies*, vol. 15, no. 7, 2022, doi: 10.3390/en15072440.
[4] “Long-term aviation fuel decarbonization: Progress, roadblocks, and policy opportunities,” *International Council on Clean Transportation*. https://theicct.org/publication/long-term-aviation-fuel-decarbonization-progress-roadblocks-and-policy-opportunities/ (accessed Sep. 15, 2022).
[5] “Waypoint 2050.” https://aviationbenefits.org/environmental-efficiency/climate-action/waypoint-2050/ (accessed Jul. 05, 2022).
[6] “FAQS,” *Synkero*. https://synkero.com/faqs/ (accessed Nov. 08, 2022).
[7] “Fact Sheet | The Growth in Greenhouse Gas Emissions from Commercial Aviation (2019) | White Papers | EESI.” https://www.eesi.org/papers/view/fact-sheet-the-growth-in-greenhouse-gas-emissions-from-commercial-aviation (accessed Apr. 28, 2022).
[8] “Global Electricity Review 2022,” *Ember*, Mar. 29, 2022. https://ember-climate.org/insights/research/global-electricity-review-2022/ (accessed Nov. 28, 2022).
[9] “Performance analysis of evolutionary hydrogen-powered aircraft,” *International Council on Clean Transportation*. https://theicct.org/publication/aviation-global-evo-hydrogen-aircraft-jan22/ (accessed Jun. 08, 2022).
[10] “Airport Compatibility - Airplane Characteristics for Aiport Planning.” https://www.boeing.com/commercial/airports/plan_manuals.page (accessed Apr. 29, 2023).
[11] B. J. Cantwell, “Fundamentals of Compressible Flow”.
[12] A. Dorsey and A. Uranga, “Design Space Exploration of Future Open Rotor Configurations,” in *AIAA Propulsion and Energy 2020 Forum*, in AIAA Propulsion and Energy Forum. American Institute of Aeronautics and Astronautics, 2020. doi: 10.2514/6.2020-3680.
[13] S. M. Jones, “An Introduction to Thermodynamic Performance Analysis of Aircraft Gas Turbine Engine Cycles Using the Numerical Propulsion System Simulation Code,” NASA/TM-2007-214690, Mar. 2007. Accessed: Oct. 20, 2022. [Online]. Available: https://ntrs.nasa.gov/citations/20070018165
[14] D. Owens, “Weissinger’s model of the nonlinear lifting-line method for aircraft design,” in *36th AIAA Aerospace Sciences Meeting and Exhibit*, American Institute of Aeronautics and Astronautics. doi: 10.2514/6.1998-597.
[15] T. W. Lukaczyk *et al.*, “SUAVE: An Open-Source Environment for Multi-Fidelity Conceptual Vehicle Design,” in *16th AIAA/ISSMO Multidisciplinary Analysis and Optimization Conference*, Dallas, TX: American Institute of Aeronautics and Astronautics, Jun. 2015. doi: 10.2514/6.2015-3087.
[16] R. S. Shevell, *Fundamentals of Flight*. Prentice-Hall, 1983.
[17] R. Shevell, *Introduction to Aircraft Design Synthesis and Analysis*. Department of Aeronautics and Astronautics, Stanford University, 1992.
[18] C. Gallagher, C. Stuart, and S. Spence, “Validation and Calibration of Conceptual Design Tool SUAVE,” *AIAA AVIATION 2023 FORUM*.
[19] C. E. Rasmussen and C. K. I. Williams, *Gaussian processes for machine learning*. in Adaptive computation and machine learning. Cambridge, Mass: MIT Press, 2006.
[20] A. Dik, N. Bitén, V. Zaccaria, I. Aslanidou, and K. G. Kyprianidis, “Conceptual Design of a 3-Shaft Turbofan Engine with Reduced Fuel Consumption for 2025,” *Energy Procedia*, vol. 142, pp. 1728–1735, Dec. 2017, doi: 10.1016/j.egypro.2017.12.556.
[21] E. Hendricks, “Development of an Open Rotor Cycle Model in NPSS Using a Multi-Design Point Approach,” 2011. doi: 10.1115/GT2011-46694.
[22] G. L. Thomas, D. E. Culley, J. L. Kratz, and K. L. Fisher, “Dynamic Analysis of the hFan, a Parallel Hybrid Electric Turbofan Engine,” in *2018 Joint Propulsion Conference*, Cincinnati, Ohio: American Institute of Aeronautics and Astronautics, Jul. 2018. doi: 10.2514/6.2018-4797.
[23] C. Perullo and D. N. Mavris, “Assessment of Vehicle Performance Using Integrated NPSS Hybrid Electric Propulsion Models,” in *50th AIAA/ASME/SAE/ASEE Joint Propulsion Conference*, in AIAA Propulsion and Energy Forum. American Institute of Aeronautics and Astronautics, 2014. doi: 10.2514/6.2014-3489.
[24] R. P. Thacker and N. Blaesser, “Modeling of a Modern Aircraft Through Calibration Techniques,” in *AIAA Aviation 2019 Forum*, in AIAA AVIATION Forum. American Institute of Aeronautics and Astronautics, 2019. doi: 10.2514/6.2019-2984.
[25] S. Vannoy and C. Cadou, “Development and Validation of an NPSS Model of a Small Turbojet Engine,” Jul. 2016. doi: 10.2514/6.2016-5063.
[26] S. M. Jones, W. J. Haller, and M. T.-H. Tong, “An N+3 Technology Level Reference Propulsion System,” E-19373, May 2017. Accessed: Aug. 09, 2022. [Online]. Available: https://ntrs.nasa.gov/citations/20170005426
[27] “Numerical Propulsion System Simulation (NPSS),” *Southwest Research Institute*, Nov. 07, 2016. https://www.swri.org/consortia/numerical-propulsion-system-simulation-npss (accessed Jun. 08, 2022).
[28] P. G. Batterton, “Energy efficient engine program contributions to aircraft fuel conservation,” presented at the Aviation Fuel Conservation Symp., Washington, DC, Jan. 1984. Accessed: Apr. 29, 2023. [Online]. Available: https://ntrs.nasa.gov/citations/19840021807
[29] “ICAO Aircraft Engine Emissions Databank,” *EASA*. https://www.easa.europa.eu/en/domains/environment/icao-aircraft-engine-emissions-databank (accessed Oct. 20, 2022).
[30] J. Huete and P. Pilidis, “Parametric study on tank integration for hydrogen civil aviation propulsion,” *International Journal of Hydrogen Energy*, vol. 46, no. 74, pp. 37049–37062, Oct. 2021, doi: 10.1016/j.ijhydene.2021.08.194.

[31] “Hydrogen-powered aviation | www.fch.europa.eu.” https://www.fch.europa.eu/publications/hydrogen-powered-aviation (accessed Jul. 05, 2022).
[32] Y. Zhou, S. Searle, and N. Pavlenko, “Current and future cost of e-kerosene in the United States and Europe”.
[33] J. Henley and J. H. E. correspondent, “European countries pledge huge expansion of North Sea wind farms,” *The Guardian*, Apr. 24, 2023. Accessed: May 12, 2023. [Online]. Available: https://www.theguardian.com/environment/2023/apr/24/european-countries-pledge-huge-expansion-of-north-sea-wind-farms
[34] E. C. M. Ruijgrok, E. J. van Druten, and B. H. Bulder, “112522 K.A. Haans MSc M.T. Marshall MTech”.
[35] “Ryanair | Results Centre.” https://investor.ryanair.com/results-centre/ (accessed Sep. 22, 2022).
[36] “Projected Costs of Generating Electricity 2020 – Analysis,” *IEA*. https://www.iea.org/reports/projected-costs-of-generating-electricity-2020 (accessed May 10, 2023).